Kardiologia Polska 2018; 76, 3: 499–509; DOI: 10.5603/KP.a2017.0248 ISSN 0022–9032

ARTYKUŁ SPECJALNY / *STATE-OF-THE-ART REVIEW*

Clinical anatomy of human heart atria and interatrial septum — anatomical basis for interventional cardiologists and electrocardiologists. Part 1: right atrium and interatrial septum

Iwona Kucybała, Katarzyna Ciuk, Wiesława Klimek-Piotrowska

Department of Anatomy, Jagiellonian University, Medical College, Krakow, Poland

INTRODUCTION

Interventional cardiology together with interventional electrocardiology are nowadays one of the fastest developing branches of medicine and latterly, indications for transcatheter interventions have been extended to more and more folded cases. In recent decades, rapid progression in treatment of various types of atrial arrhythmias, particularly atrial fibrillation and atrial flutter, has been observed. Ablation within the cavotricuspid and other parts of the right atrium, as well as cardiac resynchronisation therapy, has become a standard approach. The right atrium (RA) and the interatrial septum are not only the direct targets of various interventions but also enable access to left heart chambers. The RA consists of many unique anatomical structures whose presence and morphology not only may trigger the abnormal electric activity of the heart, but also hinder the course of procedures. Precise understanding of heart anatomy and the most frequently observed anatomical variants of atrial structures seems to be crucial for achieving satisfying results, and minimising or avoiding complications during interventional procedures.

This comprehensive summary presents in a thorough but uncomplicated way a detailed macroscopic morphology of RA and interatrial septum. It also provides the anatomical background for the most common atrial arrhythmias and invasive cardiological procedures.

RIGHT ATRIUM

Overview

The RA of the human heart is located behind the right ventricle in a rightward direction. It consists of the following parts, namely a venous component, an appendage, and a vestibule. The main body of the RA has an irregular ellipsoid shape with a triangular protrusion of the right atrial appendage from the anterolateral part. All those parts have disparate embryologic origin [1]. The interatrial septum is the part common for both atria, and its detailed anatomy and origin will be described in the next chapter.

Estimated diameters of the RA differ depending on the method of measurement. Using transcatheter echocardiography, the established normal values are: 3.4–5.3 cm (long axis) and 2.6–4.4 cm (short axis) in a four-chamber view at the end-systolic phase of the cardiac cycle along with 4.9–6.1 cm (long axis) and 4.2–5.3 cm (short axis) in a four-chamber view in the phase of maximal size of the atrium in cardiac magnetic resonance imaging. Nonetheless, currently there is a lack of clearly established standards regarding quantitative evaluation of the size of the RA, since its precise measurements are not particularly relevant to clinical practice [2].

Superior vena cava

The superior vena cava (SVC) drains into the RA on its superior wall, and its orifice is localised in the venous component of the atrium [3]. The mean diameter of the SVC orifice oscillates between 20.1 ± 3.2 mm in the mediolateral dimension and 19.2 ± 3.1 mm in the anteroposterior dimension. Previous research provided evidence that the orifice of the SVC is always deprived of any anatomical obstacles [4]. Hence, the SVC should be considered as the preferred access way during catheterisation of the RA in the majority of cases.

Terminal crest

The fibromuscular junction between the appendage and the venous component of the RA is externally marked by

---

Address for correspondence:
Wiesława Klimek-Piotrowska, MD, PhD, Department of Anatomy, Jagiellonian University, Medical College, ul. Kopernika 12, 31–034 Kraków, Poland,
e-mail: heart@cm-uj.krakow.pl

Received: 14.11.2017 **Accepted:** 15.11.2017 **Available as AoP:** 08.12.2017

Kardiologia Polska Copyright © Polskie Towarzystwo Kardiologiczne 2018

a terminal groove extending vertically between the superior and inferior caval veins. This structure corresponds to the endocardially marked muscular band known as the terminal crest [5]. The terminal crest stretches from the anteromedial wall of the RA, then it passes parallel to the anterior border of the SVC orifice, and then it curves in a posterolateral direction (Fig. 1). Close to the inferior vena cava (IVC) it bends anteriorly to get past the right border of its orifice. Subsequently, it ends its track in the region of the cavotricuspid isthmus [6–9]. The mean length of the terminal crest is 51.0 ± 9.0 mm and its thickness at the level of SVC is about 5.5 mm [10]. Occasionally, the terminal crest can be prominent, thus mimicking a right atrial mass like a pseudo mass, tumour, thrombus, or vegetation. The proximal and intercaval course of the terminal crest is quite universal in all hearts. The pattern of the ramification of the distal part of the terminal crest into the lower part of the RA varies significantly among the population, contrary to its initial and central part. Lastly, a ten-type classification of final ramifications was created. The main pattern represents one thick bundle of the distal crest, terminating in the vestibule of the tricuspid valve (type A — 25.7%), followed by many thinner bundles radiating from the distal crest beyond the cavotricuspid isthmus (type B — 15.7%), or obliquely in the cavotricuspid isthmus area in a fan-like fashion (type C — 14.3%) (Fig. 2) [9]. In about one-fifth of hearts, a second crest may be noticed, which is the pectinate muscle located medially to the terminal crest, and it ends in a discrete ridge [11].

The terminal crest plays an important role in typical atrial flutter. It provides a barrier to conduction transversely across it. The transverse conduction block by the terminal crest is more likely in thick bundles. On the other hand, fast conduction velocities can be observed in the longitudinal direction of the terminal crest [12]. About two-thirds of focal right atrial tachycardia, seen in the absence of structural heart disease, arise along the terminal crest. Ablation targeting the terminal crest has also been used in patients with inappropriate sinus tachycardia [5, 8]. Final ramifications of the crest seem to play a role in the propagation of impulses, and may have an impact on the success rate of cavotricuspid isthmus ablation. Conduction in the cavotricuspid isthmus courses preferentially along thicker bundles that could become targets for ablation where the punctual ablation of distal terminal crest ramification may result in the interruption of pathological conduction [9].

Pectinate muscles and taenia sagittalis

Pectinate muscles emerge from the terminal crest, then they extend anterolaterally on the walls of the whole right atrial appendage towards the vestibule of the RA [3]. They may present huge diversity of anatomical variants, and they can be categorised according to the classification shown in Table 1 [8]. The largest and the most prominent pectinate muscle is named taenia sagittalis (Fig. 1). In 55–65% of cases, single taenia sagittalis is present, while in 20–25% of cases more than one could be detected. In 15–20% of specimens, taenia sagittalis was absent [7, 8]. A mean length of taenia sagittalis is 12.0 mm, while its mean thickness is 0.4 mm [7].

As for the electrophysiological implications of the morphology of the appendage and its pectinate muscles, the presence of prominent trabeculations may lead to unbalanced propagation of excitatory impulses. It may be the predisposing factor to the initiation of re-entry and the prolongation of life spans of its waves, which results in severe atrial arrhythmias that may even occur in hearts with intact myocardium. Moreover, this type of pectinate muscle morphology has additional consequences for the treatment of atrial arrhythmias. During radiofrequency catheter ablation, the tip of the catheter

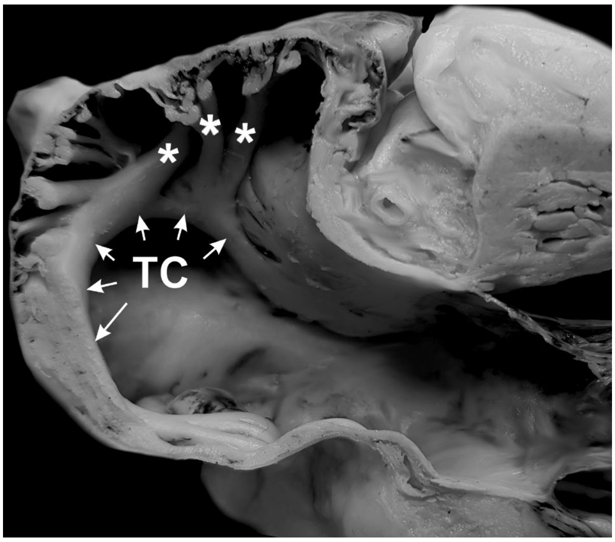

Figure 1. Lateral view of the right atrium, the right atrial appendage was dissected. Terminal crest (TC) with three taenia sagittalis (*) is marked

Table 1. Classification of the morphology of pectinate muscles. Adapted from [8]

Type	Prevalence	Description
1	40–45%	Orientation perpendicular to the terminal crest with equal spacing
2	15–18%	Orientation parallel to the terminal crest with equal spacing
3	10–11%	Combination of type 1 and 2, more than one common muscular trunk
4	9–10%	Branching of pectinate muscles
5	9–20%	Chaotic orientation, intermingling trabeculations
6	5–8%	Prominent muscular columns

may get stuck under the muscular columns and result in the perforation of the atrial wall, which may be fatal. Highly trabeculated appendages may also predispose to thrombus formation during the ablation procedure [7, 8].

Sinus node

The sinus node, the crescent-shaped natural pacemaker of the heart, is located in the proximal part of the terminal groove anterolaterally to the superior cavoatrial junction [13]. It is difficult to dissect the sinus node macroscopically. There is some evidence that an extensive "paranodal area" (rather than a well demarcated sinus node) exists in humans. The node is a more diffuse, elaborate structure, usually extending down the inferolateral aspect of the crista terminalis in a cigar shape [13–15]. The sinoatrial node artery is most commonly reported as a single vessel, originating from the right coronary artery (68.0%), and taking a retrocaval course to reach the sinus node [16]. Multiple anatomical features of the sinoatrial node are responsible for difficulties of its ablation (as may be required in patients with inappropriate sinus tachycardia). To name just a few, extensive location, close proximity of the thick crista terminalis, and the cooling effects of the nodal artery are the main obstacles [14].

Inferior vena cava, Eustachian valve, and Eustachian ridge

The orifice of the IVC is localised in the postero-inferior region of the venous part of the RA [17]. The mean dimensions of its orifice are: in the mediolateral direction 24.1 ± 5.7 mm and in the anterolateral direction 24.2 ± 5.5 mm. The mean area of the IVC orifice equals 4.8 ± 2.0 cm^2 [4]. In 1.8% of hearts, strands in the IVC orifice may be visible [4]. Muscular extensions from the atrial musculature, which encompass proximal IVC, are typically not present [18].

The Eustachian valve arises from the anterior border of the IVC orifice and typically presents as a crescentic fold of endocardium (Fig. 3A) [4]. Its embryologic origin is derived from the combination of the superior portion of the right sinus valve and the sinus septum [19]. However, in approximately 30% of cases, the valve is absent. The mean height of the Eustachian valve is about 5 mm, while the mean percentage coverage of the IVC orifice is 22.9 ± 14.6% [4, 9]. Even though in about 1.8% of cases, a prominent valve covering the whole opening of the IVC may be present, it hinders rather than enables the catheterisation of the RA and coronary sinus ostium (CSO), by directing the catheter towards the superior part of the atrium. Rarely, a giant Eustachian valve can cause obstruction of the IVC or the formation of a thrombus, and it may be an obstacle during transcatheter occlusion of patent foramen ovale. In order to minimise the risk of unforeseen complications connected with the presence of the Eustachian valve, transoesophageal or intracardiac echocardiography should be performed before the procedure. If an extensive valve is present, the use of SVC access is advised. Alternatively, the valve can be partially ablated or punctured by a needle [4].

The Eustachian ridge, which is always present, is an extension of the insertion of the Eustachian valve, which usually continues its track towards the central fibrous body, below and anteriorly to the fossa ovalis, but above the CSO (Fig. 3A, red arrows). The mean length of the Eustachian ridge is 25.5 ± 4.1 mm and the mean thickness of the ridge is 3.6 ± 1.9 mm. The thickness of the Eustachian ridge is inversely correlated with the diameter of the IVC orifice. Excessive thickening of the Eustachian ridge is quite common, with 47.9% of hearts presenting a prominent Eustachian ridge. In 9.2% of all hearts, a thick bundle of the distal terminal crest enters the Eustachian ridge [9]. Significant thickening of this structure has important implications not only for the electrophysiology of the RA, but also for endovascular procedures involving cannulation of the coronary sinus. An enlarged Eustachian ridge may create a line of fixed conduction block during typical atrial flutter. In such cases, the block of paraseptal isthmus can be achieved only after complete ablation of the excessively pronounced ridge [20]. Moreover, the prominent Eustachian ridge may form an obstacle for a catheter heading towards the CSO and cavotricuspid isthmus region, from both IVC and SVC accesses [4].

The Chiari network

The Chiari network is a net-like structure located in close proximity to the IVC orifice and CSO [21]. It is an embryologic remnant of incomplete resorption of the right sinus valve. It is visible in approximately 4.6% of hearts (Fig. 3B). Smaller holes in its structure may prevent the catheter from passing further into the atrium, while its larger compartments might restrict the range of movements of the catheter [4]. The Chiari network can easily be imaged using transthoracic echocardiography (as a highly mobile, highly reflective echo structure) [22].

Coronary sinus ostium and Thebesian valve

The coronary sinus drains into the RA postero-medially into its venous part, between the IVC and the right atrioventricular (AV) ostium [11, 23]. The mean dimension of the longest diameter of its oval-shaped ostium fluctuates around 9–15 mm [23, 24]. The excessive diameter of the CSO is considered as a risk factor of the AV nodal re-entrant tachycardia [25]. Clinically, the CSO is utilised as a passage to the left atrial and left ventricular epicardium during cardiac resynchronisation therapy, catheter ablation of cardiac arrhythmias, defibrillation, perfusion therapy, mitral valve annuloplasty, targeted drug delivery, or retrograde cardioplegia administration [23, 26]. Three elements of the CSO are related to its successful cannulation: the size of the ostium, its barriers into the RA, and the presence of a valve that may cover the ostium [4, 23, 27].

The CSO is usually covered by the Thebesian valve, which is present in 62–85% of hearts [11, 23, 28]. The valve is the

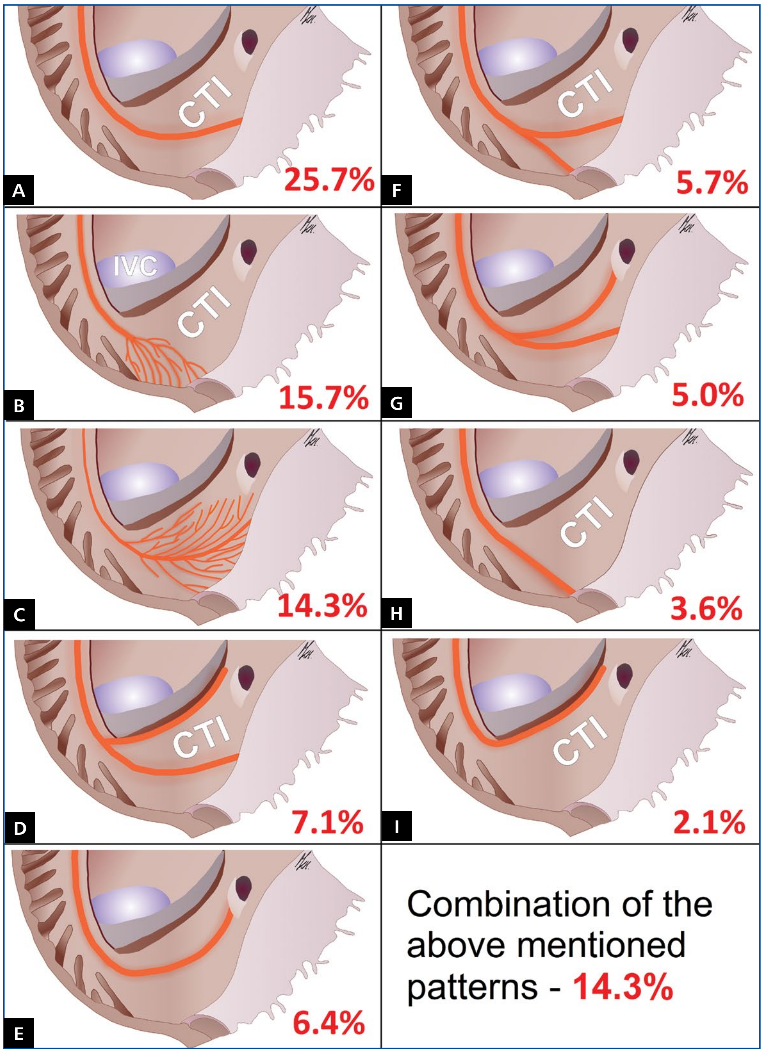
CTI
A
25.7%
F
5.7%
IVC
B
15.7%
G
5.0%
C
14.3%
H
3.6%
D
7.1%
I
2.1%
E
6.4%
Combination of the above mentioned patterns - 14.3%

Figure 2. Schematic views of the final ramifications of the distal terminal crest muscle fibres (orange) into the lower part of the right atrium; CTI — cavotricuspid isthmus; IVC — inferior vena cava. Adapted from [9]

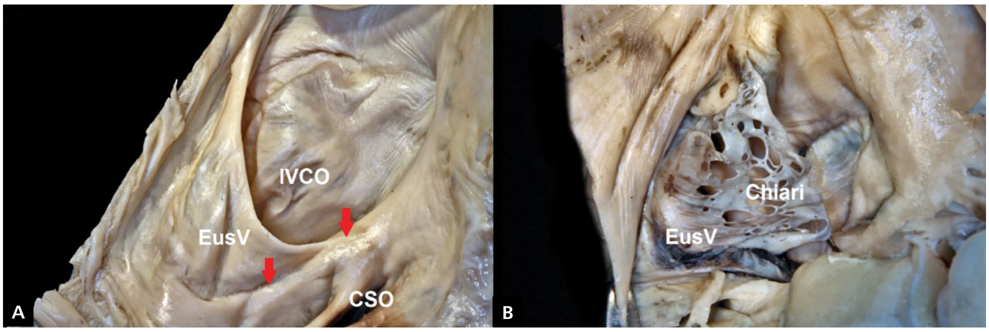
IVCO
EusV
CSO
A
Chiari
EusV
B

Figure 3. **A.** Inferior vena cava orifice (IVCO) with the Eustachian valve (EusV) present; **B.** Right atrium view with the Chiari's network; CSO — coronary sinus ostium

embryologic remnant of the inferior portion of the right sinus valve and usually has the form of an endocardial fold attached to the right border of the CSO, inferiorly to the Eustachian ridge [17, 19, 23]. The mean coverage of the CSO by the Thebesian valve is 48.3 ± 36.6% [4]. The size of the CSO is closely tied to the presence and size of the Thebesian valve.

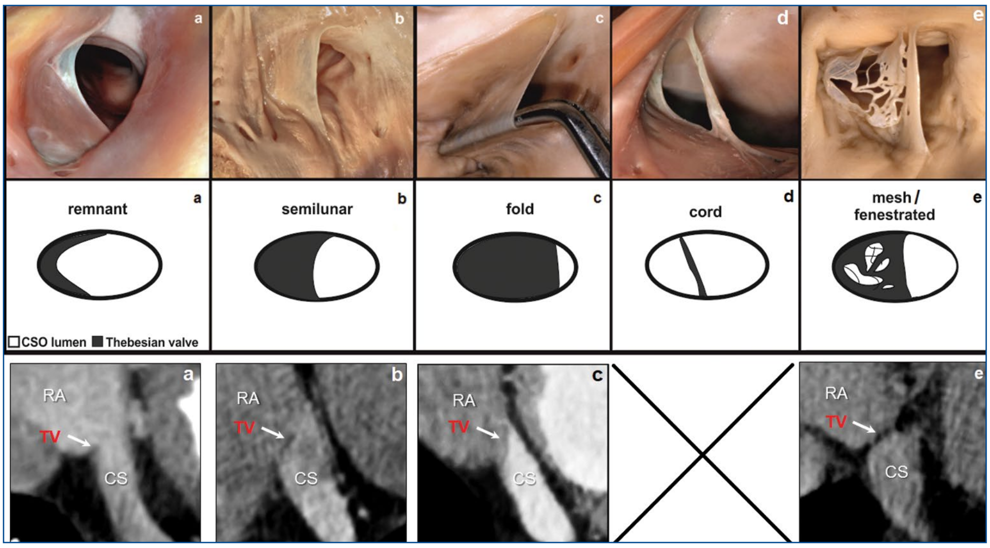

Figure 4. Types of Thebesian valve as seen in cadavers and multi-slice computed tomography: remnant (**a**); semilunar (**b**); fold (**c**); cord (**d**); mesh or fenestrated (**e**); CS — coronary sinus; CSO — coronary sinus ostium, RA — right atrium, TV — Thebesian valve. Adapted from [23] and [30]

Table 2. Classification of the morphology of the Thebesian valve. Adapted from [23] and [30]

Thebesian valve type	Name	Prevalence in cadaver material	Mean CSO coverage ± SD	H/D-ratio threshold value in MSCT	Description
I	Remnant	26%	24 ± 8%	0.00–0.35	Small hem of endocardium not protruding into CSO
II	Semilunar	33%	58 ± 11%	0.35–0.64	Semilunar fold significantly protruding into CSO
III	Fold	17%	81 ± 6%	0.64–1.00	Large, non-semilunar fold almost completely covering CSO
IV	Cord	14%	NA	NA	Single thick strand, in most cases located in CSO midline
V	Mesh or fenestrated	10%	NA	NA	Net-like valves, multiple cords or fenestrated valves of type I, II, and III

CSO — coronary sinus ostium, H/D — height/diameter; MSCT — multi-slice computed tomography, NA — not applicable, SD — standard deviation

The CSO diameter is significantly larger when the Thebesian valve is absent, compared to those accompanied by the presence of the valve. Additionally, there exists an inverse correlation between the size of the CSO and the height of the Thebesian valve. This phenomenon could be the consequence of increased blood flow in coronary sinuses of larger diameter, which lead to atrophy of the valve [23]. Moreover, when the persistent left SVC drains into the coronary sinus, the most common congenital malformation of thoracic venous return is present when the Thebesian valve is absent [29].

It has been proven that the shape and size of the Thebesian valve affects the success of coronary sinus cannulation. Five types of Thebesian valve have been distinguished, and their detailed characteristics are shown in Figure 4 and Table 2 [23, 30]. Some types of Thebesian valve morphology are especially prone to obstruction of CSO during clinical procedures. In general, "fold" type valves may significantly prolong the duration of the procedure of coronary sinus cannulation. A particularly obstructive type of Thebesian valve is the one that covers more than 100% of the ostium; this anatomic variant is seen in around 2.6% of hearts (Fig. 5). A similar percentage of failures in coronary sinus catheterisation is attributed to the inability to locate the CSO (2.87%) [31]. In such cases, because of the large fold of the valve that covers the

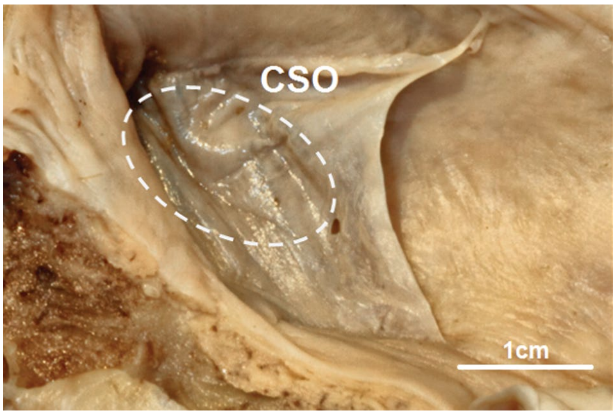

Figure 5. Obstructive Thebesian valve that covers the whole coronary sinus ostium (CSO)

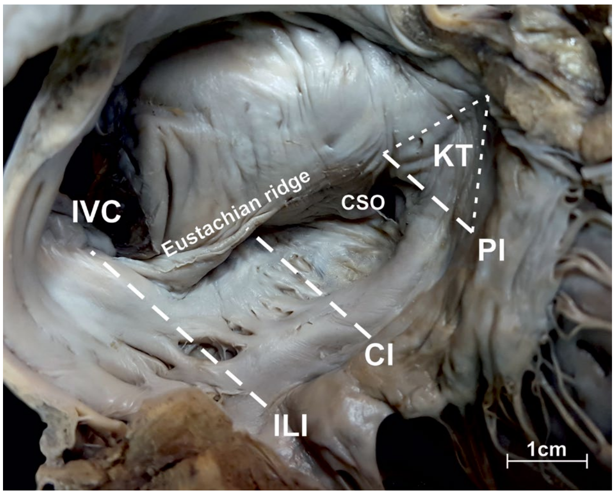

Figure 6. Cavotricuspid isthmus and Koch's triangle areas; CI — central isthmus; CSO — coronary sinus ostium; ILI — inferolateral isthmus; IVC — inferior vena cava; KT — Koch's triangle; PI — paraseptal isthmus

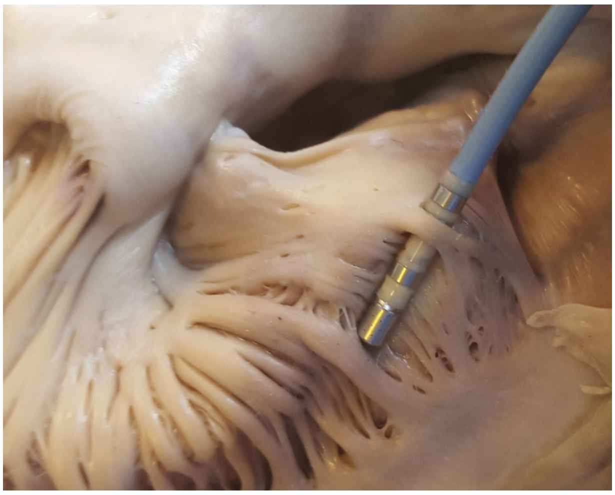

Figure 7. Cavotricuspid isthmus with muscular bridges

CSO, retrograde coronary sinus catheterisation may be completely impossible through access by either the SVC or IVC. Introduction of the catheter is unachievable not only because of the small width of the entrance under the free edge of the valve but also because of the location of the ostium behind the fold of the valve. Such location requires the insertion of the catheter under the free edge of the valve and rapid, tight rotation of more than 90° to gain access to the coronary sinus [32]. Furthermore, mesh or fenestrated valves also may hinder the procedure by limiting the range of catheter movement.

In order to prevent intraprocedural complications provoked by the morphology of the Thebesian valve, intracardiac echocardiography or left coronary angiography with levophase may be performed before the coronary sinus cannulation. If multi-slice computed tomography of the heart was performed before the procedure, it should be also utilised for the assessment of the presence and morphology of the Thebesian valve. Klimek-Piotrowska et al. [30] proposed the H/D (height/diameter) ratio as the means of evaluation of the Thebesian valve shape in computed tomography. It is calculated by dividing the Thebesian valve height by the CSO diameter. This simple method of assessment is applicable to the images obtained by 64-row detector (or higher) scanners. It does not require extensive experience in this field and should be implemented in every possible case [30]. Awareness of the presence of obstructive Thebesian valve prior to the procedure enables the modification of standard access to the CSO. The most preferable method is SVC access to the RA and then insertion of the catheter to the coronary sinus orifice on the left superior margin, rotationally moving the catheter from anterior to posterior and from the left to the right side. In the case of failure of this method, radiofrequency energy could be used to perforate the Thebesian valve.

Cavotricuspid isthmus

Cavotricuspid isthmus is a quadrilateral-shaped, usually concave area within the vestibule of the RA [9]. It is limited anteriorly by the septal tricuspid leaflet attachment and posteriorly by the Eustachian valve and ridge. The cavotricuspid isthmus is divided into three levels, namely: paraseptal isthmus (medial boundary of the cavotricuspid isthmus), central isthmus, and inferolateral isthmus (lateral boundary of the cavotricuspid isthmus). Paraseptal isthmus (or septal isthmus, or Koch's triangle base) is defined as the line between the left end of the Eustachian ridge and the tricuspid annulus, tangent to the left contour of the CSO. The central isthmus (or inferior isthmus) is characterised as the line limited by the midpoint of the Eustachian ridge and the septal leaflet of the tricuspid valve, parallel to the paraseptal isthmus. The inferolateral isthmus is defined as the line between the right end of the Eustachian ridge and the right end of the septal leaflet of the tricuspid valve, parallel to the paraseptal and central isthmus (Fig. 6) [9, 33].

The mean lengths of the paraseptal, central, and inferolateral isthmus are: 18.5 ± 4.0 mm, 24.0 ± 4.2 mm, and 29.3 ± 4.9 mm, respectively. In the space between the paraseptal isthmus and central isthmus, the CSO and sub-Eustachian recesses are located. The sub-Eustachian recess is also known as the sub-Thebesian recess/sinus or sinus of Keith [9]. A single sub-Eustachian recess occur in 48.6% of hearts, while a double recess is present in 2.9% of hearts. Moreover, the space between the inferolateral and central isthmus is divided into three parts: anterior (smooth-walled), middle (simply trabeculated or with the presence of intratrabecular recesses or trabecular bridges), and posterior sector (membranous) [9, 34].

As for the clinical significance of this area, the isthmus-dependent variant of atrial flutter is most prevalent in the population. In this form, the macro–re-entrant circuit stretches around the tricuspid annulus in a counter-clockwise manner [3]. Hence, cavotricuspid isthmus ablation is the treatment of choice for typical atrial flutter. Proper selection of the ablation site is crucial for positive results of the procedure without occurrence of intraprocedural complications. The paraseptal isthmus was found to be the shortest, and thus theoretically it should be considered as a preferable ablation site. However, this logic is incorrect due to the fact that ablation difficulties are not typically caused by isthmus length, but instead are caused by the anatomical location, tissue thickness, pouches, or muscular ridges or trabeculae.

Ablation of the paraseptal isthmus (base of the Koch triangle, Fig. 6) should be avoided because it may lead to damage of the AV node, and complete block of conduction may occur. Also, the muscular layer in this region is the thickest in the whole cardiotricuspid isthmus, and the substantial amount of energy required for ablation here poses an even greater risk of AV node injury [9, 35]. Due to possible clinical impairments, the inferolateral and central isthmuses are considered to be better places for ablation. Nevertheless, the presence of the sub-Eustachian recess within the central isthmus limits the effectiveness of ablation in this site and may prolong ablation and increase the complication risk. Moreover, it should be taken into account that the distance between the endocardial surface of the central isthmus and the right coronary artery ranges from 2 mm to 11 mm [18]. The presence of intertrabecular recesses (25.0%), trabecular bridges (12.9%), and sub-Eustachian recesses within the cavotricuspid isthmus can also make ablation more difficult. Muscular bridges that are parallel to the isthmus may hinder the catheter between the tissue bridge and the thin atrial wall (Fig. 7). In addition, because of gaps between the bridges and the proper atrial wall, the amount of energy needed to achieve the isthmus block in this anatomic variant might be significantly higher [9]. Hence, thorough assessment of the cavotricuspid isthmus anatomy should be done before each ablation procedure, preferably with use of transthoracic, transoesophageal, or intracardiac echocardiography. Additionally, computed tomography or magnetic resonance imaging of the heart could be used for this purpose, if it was performed before the procedure.

Koch’s triangle and AV node

Koch’s triangle, which is the part of the vestibule of the RA, is considered as an anatomic landmark for the localisation of the AV node. The borders of Koch’s triangle have recently been redefined. Its apex is located in the central fibrous body and is the site of penetration of the bundle of His, while its base is identical to the paraseptal isthmus and is described as the line segment tangent to the left border of the CSO between the left end of the Eustachian ridge and the tricuspid annulus. The anterior edge of the triangle stretches between the apex and the point where the base touches the tricuspid annulus. The posterior edge extends between the apex and the point where the base reaches left end of the Eustachian ridge (Fig. 6) [36]. Previous studies equated the posterior edge with the tendon of Todaro — the part of the fibrous skeleton of the heart located in the subendocardium, which runs between the left end of the Eustachian ridge and the central fibrous body. Nonetheless, this structure could be identified only microscopically in adults, and thus this concept is not useful for clinical practice. As for the mean dimensions, the length of the base, anterior edge and posterior edge are: 18.5 ± 4.0 mm, 18.0 ± 3.8 mm, and 20.3 ± 4.3 mm, respectively, and the mean triangle height (apex to the base) is 16.0 ± 3.7 mm. However, its size is highly variable between individuals. Also, attempts to create a mathematical formula that enables calculation of Koch’s triangle size in adults relating to the measurements of the body habitus or intracardiac morphometric parameters were completely unsuccessful [36].

The AV node is found mainly at the Koch’s triangle apex. The node is quite compact (1 × 3 × 5 mm), but is surrounded by area of transitional cardiomyocytes. The compact part of the AV node could be found beneath the atrial surface of the central fibrous body and its right extension lies closely to the tricuspid annulus. Moreover, the distance between the endocardial surface of the base of Koch’s triangle and the artery supplying the AV node is 3.5 ± 1.5 mm [37]. Most frequently the AV nodal branch arises as a distal branch from the right coronary artery near the crux of the heart (80%). Knowledge of Koch’s triangle dimensions is extremely important to safely perform radio-frequency catheter ablation within the RA because unwanted ablation of the AV node inside Koch’s triangle may result in nodal injury and complete block of conduction. On the other hand, the area of Koch’s triangle is related to the pathophysiology of AV nodal re-entrant tachycardias. Hence, the musculature located in the apex of the Koch’s triangle is not the target for ablation of the so-called fast pathway. However, the base of the triangle is often used as an ablation site for the slow pathway of nodal re-entrant tachycardia along with inferior paraseptal, septal, and superior paraseptal accessory pathways and other arrhythmias arising from that

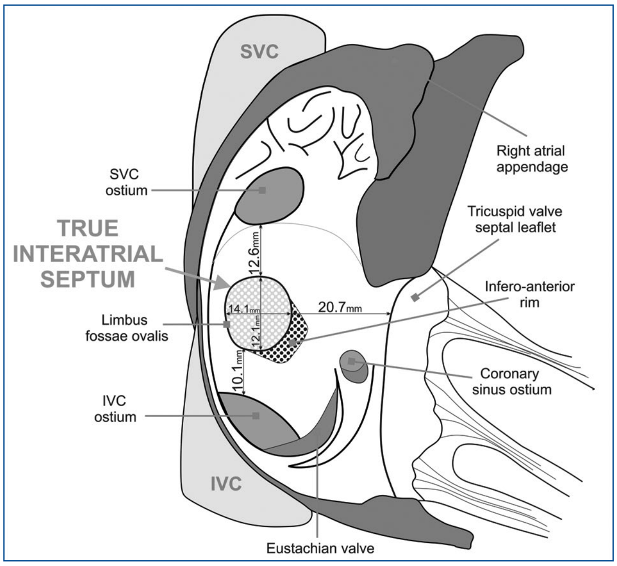

Figure 8. Right atrial view of the interatrial septum. Stippled area represents the true interatrial septum; IVC — inferior vena cava; SVC — superior vena cava. Adapted from [42]

localisation [38]. Also, the region adjacent to the base of the triangle is a possible spot for ablation of isthmus-dependent atrial flutter, but this is not advised (cavotricuspid isthmus) [9].

Right phrenic nerve

The right phrenic nerve passes anteriorly to the subclavian artery, and posteriorly to the subclavian vein. It enters the thorax via the superior thoracic aperture, then descends anteriorly to the right lung root, vertically along the SVC, down on the right side of the pericardium along the RA, and over the lateral aspect of the terminal segment of the IVC [39]. The average distance from the sinus node to the right phrenic nerve is 3.2–10.2 mm, so ablation procedures in this area should be undertaken with extreme caution [40, 41]. Furthermore, the inferolateral isthmus is located close to the course of the right phrenic nerve, and ablation in that region might lead to its damage.

INTERATRIAL SEPTUM

Overview

Clinical anatomy of the interatrial septum may seem simple, but it is thoroughly insidious, tough, and laborious to describe. Its unacquaintance may result in severe complications. The position of the RA and its correlation with the left atrium constitute the location of the interatrial septum. The left atrium is placed posteriorly and relatively superiorly to the RA, and the dividing structure (the septal plane) determines the angle with the median sagittal plane when observed from the front of the thorax. The right anterior oblique projection can show the septal plane *en face* [18, 42].

Analysing the morphology of the septum from the side of the RA, the fossa ovalis and adjacent muscular rim (limbus) are its main components. The floor of the fossa ovalis derives from embryologic septum primum. The superior part of the rim forms infolding of the atrial wall between the venous part of the RA and right pulmonary veins. This structure is visible from the outside of the heart as a groove filled with epicardial fat (termed as Waterson's groove), which often contains the artery supplying the sinus node [3].

True interatrial septum

The interatrial septum and the true interatrial septum (clinically significant) are two different, often mistaken, concepts. The traditionally comprehended interatrial septum is a fibro-muscular area interposed between atria and limited anteriorly by the right AV ring, antero-inferiorly by the CSO, inferiorly by the IVC orifice, posteriorly by folds of the atrial wall, superiorly by the SVC orifice, and antero-superiorly by the non-coronary sinus of Valsalva [43]. This area is known as the 'false' interatrial septum. Dissections and transections reveal that a very small part of the mentioned area can be removed without opening the right atrial wall [42]. The true interatrial septum is a smaller area, which could be excised without perforating the external wall of the heart. It constitutes about 20% of the 'false' interatrial septum area (Fig. 8). Only the floor of the fossa ovalis and its direct infero-anterior rim build the true septum between the atria. The superior, antero-superior, and posterior rims are created by infoldings of the adherent right and left atrial walls and do not form the true interatrial septum [44]. This has direct clinical transfer because the transseptal puncture could be safely performed only within the borders of the true interatrial septum [42].

The fossa ovalis is an oval or round concavity in the infero-posterior part of the interatrial septum and is composed mainly of thin fibrous tissue. The mean anteroposterior and craniocaudal diameters of the fossa are: 14.1 ± 3 .6 mm and 12.1 ± 3.6 mm, respectively, while the mean area of the fossa ovalis measures 142.7 ± 65.0 mm^2, and its dimensions increase with age. There are four variations of fossa ovalis anatomy when we are looking from the right atrial side: 'smooth' fossa ovalis (56%), patent foramen ovale (PFO) channel (25%), right-sided septal pouch (11%), and net-like formation within the fossa ovalis (7%). When looking from the left atrial side, the smooth septum, PFO channel, and left-sided SP may be observed [42].

Patent foramen ovale channel

The fossa ovalis valve opens leftward during the foetal life and enables communication between the right and left atrium. Physiologically, the communication closes within the first two years of life. The PFO is observed in about 10–35% of the general population; it is a persistence of foetal interatrial connection [45]. In the vast majority of cases, the PFOs have

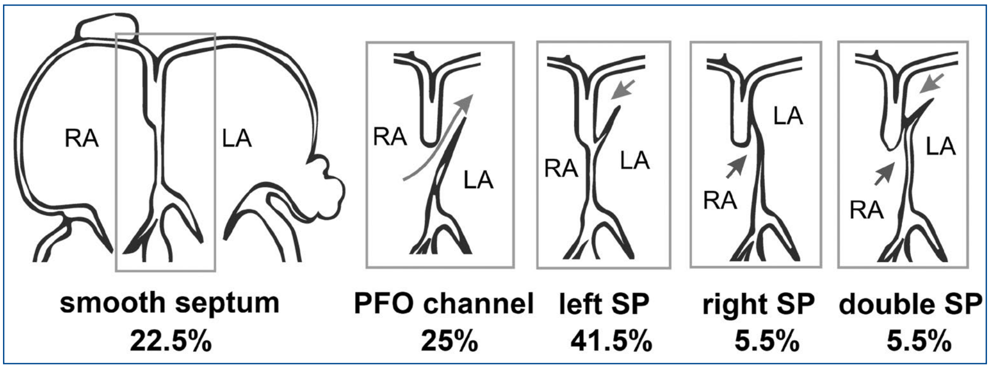

Figure 9. Schematic view of the interatrial septum; LA — left atrium; PFO — patent foramen ovale; RA — right atrium; SP — septal pouch. Adapted from [46]

the form of a channel that is built by the non-adherent flap valve of the septum and the surrounding rims of the fossa ovalis. The PFO is located at the area of the embryonic septum secundum and mainly situated in the central part of the superior circumference of the fossa ovalis. The diameter of PFO opening varies from 1 mm to 19 mm (mean 4.9 mm), and the average size increases with each decade of life [45]. The PFO mean channel length is about 10 mm. The tunnel-like PFO (channel length ≥ 12 mm) is observed in 8.9% of specimens [42]. The frequency of PFO is higher in young adults compared to elderly people, which suggests a tendency for its fusion with age [45, 46].

The PFO plays a significant role in the pathogenesis of cardioembolic stroke. Two main mechanisms are postulated: paradoxical embolisation and in situ thrombus formation within the PFO channel or on the left side of the septum (especially when the atrial septal aneurysm is present). It was proven that some of the anatomical features of the PFO may be associated with greater risk of stroke. Larger PFOs, longer channels, larger interatrial shunt, and a greater frequency of atrial septal aneurysm are morphological features of the septum, which increase the probability of stroke. Moreover, some of the right atrial features, such as embryological remnants including a Chiari network and prominent Eustachian valve, may increase stroke risk [47].

Atrial septal pouch

Atrial SP is a recently re-described anatomical entity that can be defined as a diverticulum within the interatrial septum (Fig. 9) [46]. This morphological concept was introduced by Krishnan and Salazar in 2010 and developed by Hołda et al. in 2016 [46, 48]. The SP may be located either on the right or on the left side of the septum, or coexistence of two pouches on both sides of the septum without any connection between atria may be found. The septal pouches are formed as a result of the incomplete fusion of the PFO channel when the septum primum and septum secundum are partially fused. No coexistence of the PFO channel and SP is possible. Constant friction between human PFO channel walls leads to its natural closure, but the result of this process depends on the location of the point of adhesion. Lifelong remodelling of the interatrial septum may lead to creation of the atrial septal pouches or smooth septum. When the PFO has a short channel, fusion is completed and results in the development of a smooth septum at an early age. A long channel may fuse with the remaining part of the septum at three different levels: caudal, central, or cranial. The right SP (5.5% of all hearts) exists when the fusion is limited to the cranial portion of the zone of overlap, while the left SP (41.5% of all hearts) occurs when the fusion is limited to the caudal part of the zone of overlap. Fusion of the central portion of the zone of overlap leads to a double SP (5.5% of all hearts) [42, 46]. The term "left-sided SP" describes a pouch located on the left side of the interatrial septum (left and double), while the "right-sided SP" is used when the pouch is present on the right side of the septum (right and double). The high prevalence of SPs (over 50% of the healthy population) indicates that the pouch is not a pathology but instead is an element of normal human anatomy.

The right-sided SP is restricted from the right side by the antero-superior rim and from the left side by the floor of the fossa ovalis. Its apex is directed upward and forward. The mean depth of the right-sided SP is 6.2 ± 3.4 mm. This structure seems to play no clinical role.

The left-sided SP is located at the junction of the left side of the interatrial septum and the left atrium anterior wall, and it is built by free wall, cavity, and the atrial wall. The apex of the left-sided SP is oriented downward, and the ostium is positioned at an angle of 10–50° towards the left. The left-sided SP depth is about 8.4 ± 5.1 mm and its mean volume is 0.31 ± 0.11 mL [46]. The free wall of left-sided SP is composed of two layers of endocardium, between which transverse muscle fibres and connective tissue can be found. The atrial wall of the SP is morphologically typical of an atrium.

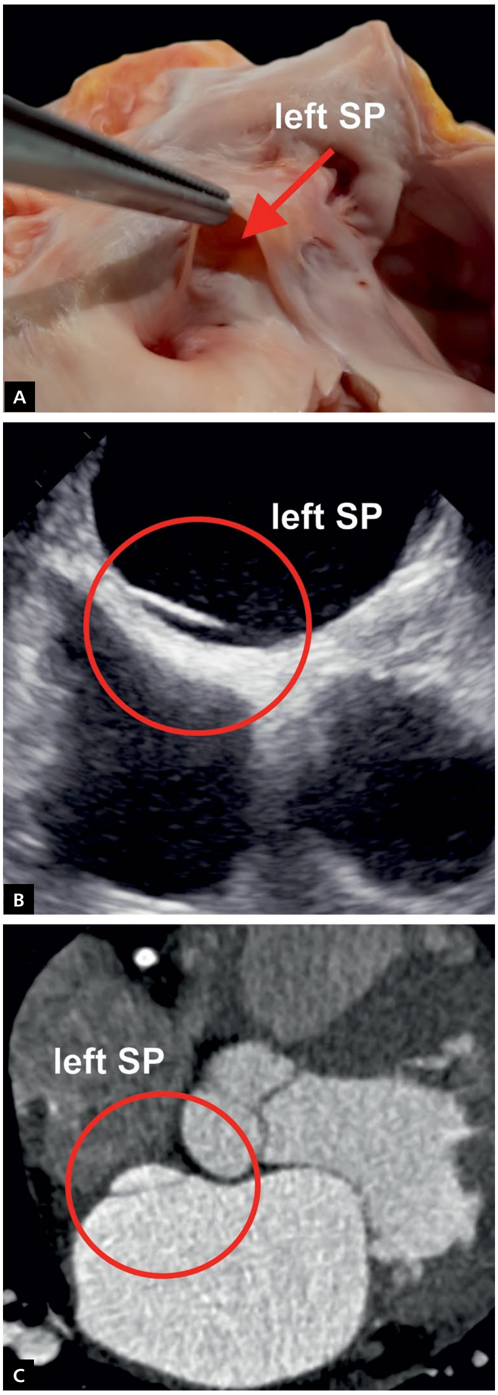

Figure 10. Left septal pouch (SP) as seen in (A) cadavers, (B) transoesophageal echocardiography, and (C) multi-slice computed tomography

The morphology of the left-sided SP is thoroughly described; however, the clinical significance of this structure remains unclear [46]. Shortly after the SP concept came to light, over a dozen case reports noted that pouches located on the left side of the interatrial septum may be the site of origin of thrombus formation and the source of ischaemic strokes. The anatomy of left-sided SP may promote blood stasis and thrombus formation; however, despite some evidence, in preliminary epidemiologic retrospective studies of left-sided pouch involvement in the pathogenesis of cardio-embolic stroke the association between the SP and cryptogenic stroke remains controversial [49]. Further studies are necessary to validate a possible relationship between the left-sided SP and cerebrovascular accidents. In addition, the left-sided SP may be a trigger for atrial fibrillation because it was recently proven that the presence of this structure is associated with increased risk of atrial fibrillation [50]. Due to the potential clinical significance of left-sided SP, its routine evaluation should not be neglected, particularly in patients with cryptogenic stroke, for whom the SP should be thoroughly investigated using transoesophageal echocardiography or multi-slice computed tomography (Fig. 10).

Conflict of interest: *none declared*

References

1. Farré J, Anderson RH, Cabrera JA, et al. Cardiac anatomy for the interventional arrhythmologist: I.terminology and fluoroscopic projections. Pacing Clin Electrophysiol. 2010; 33(4): 497–507, doi: 10.1111/j.1540-8159.2009.02644.x, indexed in Pubmed: 20059709.
2. Malik SB, Kwan D, Shah AB, et al. The right atrium: gateway to the heart--anatomic and pathologic imaging findings. Radiographics. 2015; 35(1): 14–31, doi: 10.1148/rg.351130010, indexed in Pubmed: 25590385.
3. Faletra FF, Pandian NG, Ho SY. Anatomy of the Heart by Multislice Computed Tomography. Wiley-Blackwell, Oxford 2008.
4. Klimek-Piotrowska W, Hołda MK, Koziej M, et al. Anatomical barriers in the right atrium to the coronary sinus cannulation. PeerJ. 2016; 3: e1548, doi:10.7717/peerj.1548, indexed in Pubmed: 26823994.
5. Sánchez-Quintana D, Anderson RH, Cabrera JA, et al. The terminal crest: morphological features relevant to electrophysiology. Heart. 2002; 88(4): 406–411, doi: 10.1136/heart.88.4.406, indexed in Pubmed: 12231604.
6. Rastogi R, Budhiraja V, Jain SK, et al. Morphological pattern of Crista terminalis, Musculi pectinati and Taenia sagittalis with applied significance. J Morphol Sci. 2016; 33(3): 142–145, doi: 10.4322/jms.092015.
7. Loukas M, Tubbs RS, Tongson JM, et al. The clinical anatomy of the crista terminalis, pectinate muscles and the teniae sagittalis. Ann Anat. 2008; 190(1): 81–87, doi: 10.1016/j.aanat.2007.05.002, indexed in Pubmed: 18342146.
8. Siddiqui AU, Daimi SR, Gandhi KR, et al. Crista terminalis, musculi pectinati, and taenia sagittalis: anatomical observations and applied significance. ISRN Anat. 2013; 2013: 803853, doi: 10.5402/2013/803853, indexed in Pubmed: 25938104.
9. Klimek-Piotrowska W, Hołda MK, Koziej M, et al. Clinical Anatomy of the Cavotricuspid Isthmus and Terminal Crest. PLoS One. 2016; 11(9): e0163383, doi: 10.1371/journal.pone.0163383, indexed in Pubmed: 27682030.
10. Matsuyama Ta, Inoue S, Kobayashi Y, et al. Anatomical diversity and age-related histological changes in the human right atrial posterolateral wall. Europace. 2004; 6(4): 307–315, doi: 10.1016/j.eupc.2004.03.011, indexed in Pubmed: 15172655.
11. Gami AS, Edwards WD, Lachman N, et al. Electrophysiological anatomy of typical atrial flutter: the posterior boundary and causes for difficulty with ablation. J Cardiovasc Electrophysiol. 2010; 21(2): 144–149, doi: 10.1111/j.1540-8167.2009.01607.x, indexed in Pubmed: 19804553.
12. Saffitz JE, Kanter HL, Green KG, et al. Tissue-specific determinants of anisotropic conduction velocity in canine atrial and ventricular myocardium. Circ Res. 1994; 74(6): 1065–1070, doi: 10.1161/01.res.74.6.1065, indexed in Pubmed: 8187276.
13. Monfredi O, Dobrzynski H, Mondal T, et al. The anatomy and physiology of the sinoatrial node--a contemporary review. Pacing Clin Electrophysiol. 2010; 33(11): 1392–1406, doi: 10.1111/j.1540-8159.2010.02838.x, indexed in Pubmed: 20946278.

14. Sánchez-Quintana D, Cabrera JA, Farré J, et al. Sinus node revisited in the era of electroanatomical mapping and catheter ablation. Heart. 2005; 91(2): 189–194, doi: 10.1136/hrt.2003.031542, indexed in Pubmed: 15657230.
15. Chandler NJ, Greener ID, Tellez JO, et al. Molecular architecture of the human sinus node: insights into the function of the cardiac pacemaker. Circulation. 2009; 119(12): 1562–1575, doi: 10.1161/CIRCULATIONAHA.108.804369, indexed in Pubmed: 19289639.
16. Vikse J, Henry BM, Roy J, et al. Anatomical Variations in the Sinoatrial Nodal Artery: A Meta-Analysis and Clinical Considerations. PLoS One. 2016; 11(2): e0148331, doi: 10.1371/journal.pone.0148331, indexed in Pubmed: 26849441.
17. Anderson RH, Cook AC. The structure and components of the atrial chambers. Europace. 2007; 9 Suppl 6: vi3–vi9, doi: 10.1093/europace/eum200, indexed in Pubmed: 17959691.
18. Ho SY, Sabine E. Anatomy for cardiac electrophysiologists: a practical handbook. Cardiotext Publishing 2012.
19. Steding G, Xu JW, Seidl W, et al. Developmental aspects of the sinus valves and the sinus venosus septum of the right atrium in human embryos. Anat Embryol (Berl). 1990; 181(5): 469–475, doi: 10.1007/bf02433794, indexed in Pubmed: 2372133.
20. Chang SL, Tai CT, Lin YJ, et al. The electroanatomic characteristics of the cavotricuspid isthmus: implications for the catheter ablation of atrial flutter. J Cardiovasc Electrophysiol. 2007; 18(1): 18–22, doi: 10.1111/j.1540-8167.2006.00647.x, indexed in Pubmed: 17081213.
21. Islam AK, Sayami LA, Zaman S. Chiari network: A case report and brief overview. J Saudi Heart Assoc. 2013; 25(3): 225–229, doi:10.1016/j.jsha.2012.12.002, indexed in Pubmed: 24174864.
22. Teo EYL, Ittleman F, Hamlin MP. A Chiari network and difficult cannulation of the coronary sinus for retrograde perfusion. Anesth Analg. 2010; 111(1): 79–81, doi: 10.1213/ANE.0b013e3181e05329, indexed in Pubmed: 20519420.
23. Hołda MK, Klimek-Piotrowska W, Koziej M, et al. Anatomical variations of the coronary sinus valve (Thebesian valve): implications for electrocardiological procedures. Europace. 2015; 17(6): 921–927, doi: 10.1093/europace/euu397, indexed in Pubmed: 25767087.
24. Ghosh SK, Raheja S, Tuli A. Obstructive Thebesian valve: anatomical study and implications for invasive cardiologic procedures. Anat Sci Int. 2014; 89(2): 85–94, doi: 10.1007/s12565-013-0203-0, indexed in Pubmed: 24043316.
25. Ezhumalai B, Satheesh S, Anantha A, et al. Coronary sinus diameter by echocardiography to differentiate atrioventricular nodal reentrant tachycardia from atrioventricular reentrant tachycardia. Cardiol J. 2014; 21(3): 273–278, doi: 10.5603/CJ.a2013.0088, indexed in Pubmed: 23799560.
26. Mlynarski R, Mlynarska A, Tendera M, et al. Coronary sinus ostium: the key structure in the heart's anatomy from the electrophysiologist's point of view. Heart Vessels. 2011; 26(4): 449–456, doi: 10.1007/s00380-010-0075-3, indexed in Pubmed: 21240507.
27. Mazur M, Hołda M, Koziej M, et al. Morphology of tributaries of coronary sinus in humans - corrosion casting study. Folia Med Cracov. 2015; 55(2): 5–13, indexed in Pubmed: 26839238.
28. Hellerstein HK, Orbison JL. Anatomic variations of the orifice of the human coronary sinus. Circulation. 1951; 3(4): 514–523, doi: 10.1161/01.cir.3.4.514, indexed in Pubmed: 14822159.
29. Tyrak KW, Holda J, Holda MK, et al. Persistent left superior vena cava. Cardiovasc J Afr. 2017; 28(3): e1–e4, doi: 10.5830/CVJA-2016-084, indexed in Pubmed: 28759082.
30. Klimek-Piotrowska W, Koziej M, Hołda MK, et al. The Thebesian valve height/coronary sinus ostium diameter ratio (H/D-Ratio) as a new indicator for specifying the morphological shape of the valve itself in multisliced computed tomography. Int J Cardiol. 2015; 201: 595–600, doi:10.1016/j.ijcard.2015.08.144, indexed in Pubmed: 26340123.
31. Azizi M, Castel MA, Behrens S, et al. Experience with coronary sinus lead implantations for cardiac resynchronization therapy in 244 patients. Herzschrittmacherther Elektrophysiol. 2006; 17(1): 13–18, doi: 10.1007/s00399-006-0502-4, indexed in Pubmed: 16547655.
32. Holda MK, Koziej M, Klimek-Piotrowska W. Thebesian valve: the cause of unsuccessful retrograde coronary sinus cannulation. Anatol J Cardiol. 2015; 15(3): E8–E9, doi: 10.5152/akd.2015.5952, indexed in Pubmed: 25880190.
33. Saremi F, Pourzand L, Krishnan S, et al. Right atrial cavotricuspid isthmus: anatomic characterization with multi-detector row CT. Radiology. 2008; 247(3): 658–668, doi: 10.1148/radiol.2473070819, indexed in Pubmed: 18487534.
34. Cabrera JA, Sanchez-Quintana D, Ho SY, et al. The architecture of the atrial musculature between the orifice of the inferior caval vein and the tricuspid valve: the anatomy of the isthmus. J Cardiovasc Electrophysiol. 1998; 9(11): 1186–1195, doi: 10.1111/j.1540-8167.1998.tb00091.x, indexed in Pubmed: 9835263.
35. Cabrera JA, Sánchez-Quintana D, Farré J, et al. The inferior right atrial isthmus: further architectural insights for current and coming ablation technologies. J Cardiovasc Electrophysiol. 2005; 16(4): 402–408, doi: 10.1046/j.1540-8167.2005.40709.x, indexed in Pubmed: 15828885.
36. Klimek-Piotrowska W, Holda MK, Koziej M, et al. Geometry of Koch's triangle. Europace. 2017; 19(3): 452–457, doi: 10.1093/europace/euw022, indexed in Pubmed: 27247009.
37. Sánchez-Quintana D, Ho SY, Cabrera JA, et al. Topographic anatomy of the inferior pyramidal space: relevance to radiofrequency catheter ablation. J Cardiovasc Electrophysiol. 2001; 12(2): 210–217, doi: 10.1046/j.1540-8167.2001.00210.x, indexed in Pubmed: 11232621.
38. Sánchez-Quintana D, Pizarro G, López-Mínguez JR, et al. Standardized review of atrial anatomy for cardiac electrophysiologists. J Cardiovasc Transl Res. 2013; 6(2): 124–144, doi: 10.1007/s12265-013-9447-2, indexed in Pubmed: 23389853.
39. Berkmen YM, Davis SD, Kazam E, et al. Right phrenic nerve: anatomy, CT appearance, and differentiation from the pulmonary ligament. Radiology. 1989; 173(1): 43–46, doi: 10.1148/radiology.173.1.2781029, indexed in Pubmed: 2781029.
40. Ho SY, Sánchez-Quintana D. Anatomy and pathology of the sinus node. J Interv Card Electrophysiol. 2016; 46(1): 3–8, doi: 10.1007/s10840-015-0049-6, indexed in Pubmed: 26319648.
41. Sánchez-Quintana D, Cabrera JA, Climent V, et al. How close are the phrenic nerves to cardiac structures? Implications for cardiac interventionalists. J Cardiovasc Electrophysiol. 2005; 16(3): 309–313, doi: 10.1046/j.1540-8167.2005.40759.x, indexed in Pubmed: 15817092.
42. Klimek-Piotrowska W, Hołda MK, Koziej M, et al. Anatomy of the true interatrial septum for transseptal access to the left atrium. Ann Anat. 2016; 205: 60–64, doi: 10.1016/j.aanat.2016.01.009, indexed in Pubmed: 26879344.
43. Sweeney LJ, Rosenquist GC. The normal anatomy of the atrial septum in the human heart. Am Heart J. 1979; 98(2): 194–199, doi: 10.1016/0002-8703(79)90221-7, indexed in Pubmed: 453022.
44. Anderson R, Webb S, Brown N. Clinical anatomy of the atrial septum with reference to its developmental components. Clin Anat. 1999; 12(5): 362–374, doi: 10.1002/(sici)1098-2353(1999)12:5<362::aid-ca6>3.0.co;2-f, indexed in Pubmed: 10462733.
45. Hagen PT, Scholz DG, Edwards WD. Incidence and size of patent foramen ovale during the first 10 decades of life: an autopsy study of 965 normal hearts. Mayo Clin Proc. 1984; 59(1): 17–20, doi: 10.1016/s0025-6196(12)60336-x, indexed in Pubmed: 6694427.
46. Hołda MK, Koziej M, Hołda J, et al. Atrial septal pouch - Morphological features and clinical considerations. Int J Cardiol. 2016; 220: 337–342, doi:10.1016/j.ijcard.2016.06.141, indexed in Pubmed: 27390952.
47. Homma S, Messé SR, Rundek T, et al. Patent foramen ovale. Nat Rev Dis Primers. 2016; 2: 15086, doi: 10.1038/nrdp.2015.86, indexed in Pubmed:27188965.
48. Gurudevan SV, Shah H, Tolstrup K, et al. Septal thrombus in the left atrium: is the left atrial septal pouch the culprit? JACC Cardiovasc Imaging. 2010; 3(12): 1284–1286, doi: 10.1016/j.jcmg.2010.10.003, indexed in Pubmed: 21163458.
49. Strachinaru M, Castro-Rodriguez J, Verbeet T, et al. The left atrial septal pouch as a risk factor for stroke: A systematic review. Arch Cardiovasc Dis. 2017; 110(4): 250–258, doi: 10.1016/j.acvd.2017.01.001, indexed in Pubmed: 28236567.
50. Hołda MK, Koziej M, Wszołek K, et al. Left atrial accessory appendages, diverticula, and left-sided septal pouch in multi-slice computed tomography. Association with atrial fibrillation and cerebrovascular accidents. Int J Cardiol. 2017; 244: 163–168, doi: 10.1016/j.ijcard.2017.06.042, indexed in Pubmed: 28629626.

Cite this article as: Kucybała I., Ciuk K, Klimek-Piotrowska W. Clinical anatomy of human heart atria and interatrial septum — anatomical basis for interventional cardiologists and electrocardiologists. Part 1: right atrium and interatrial septum. Kardiol Pol. 2018; 76(3): 499–509, doi: 10.5603/KP.a2017.0248.